

$^{58}\text{Ni}(\vec{p}, p')$ reaction at 60 MeV: Study of the analyzing power for inelastic excitation of the giant resonance region of the nuclear continuum and of low-lying bound states*

D. C. Kocher, F. E. Bertrand, E. E. Gross, and E. Newman

Oak Ridge National Laboratory, Oak Ridge, Tennessee 37830

(Received 7 July 1976)

The analyzing power of the giant resonance region of the nuclear continuum and of low-lying bound states for incident 60-MeV polarized protons has been investigated in the $^{58}\text{Ni}(\vec{p}, p')$ reaction. The measurements are compared with collective-model distorted-wave Born-approximation calculations employing a spin-orbit transition potential of the full-Thomas form and optical-model parameters which give a good description of the analyzing power for proton elastic scattering from ^{58}Ni at 60 MeV. The predicted analyzing powers for the giant quadrupole ($E2$) resonance at $E_x = 16.5$ MeV and for low-lying bound states with $J^\pi = 2^+, 3^-,$ and 4^+ are in qualitative agreement with the measurements for $\theta_{\text{lab}} = 15\text{--}60^\circ$. However, a systematic discrepancy is observed for the quadrupole resonance, where the measurements for $\theta_{\text{lab}} = 15\text{--}30^\circ$ are considerably more negative than the calculations. A similar but less pronounced effect is observed for the strongly excited 2^+ and 3^- bound states. Improved fits to the analyzing power for the quadrupole resonance are obtained by reducing the spin-orbit diffuseness parameter or by including an attractive imaginary spin-orbit potential. Analysis of the cross section for a weaker resonance at $E_x = 13.5$ MeV indicates an $E2$ assignment. The analyzing power for the unstructured nuclear continuum above the giant resonance region is $A_y \approx -0.05 \pm 0.01$ at most angles between 15 and 40° .

NUCLEAR REACTIONS $^{58}\text{Ni}(\vec{p}, p)$, (\vec{p}, p') , $E_p = 60.2$ MeV, $E_x = 0\text{--}31$ MeV; measured cross section $\sigma(E_x, \theta)$, analyzing power $A_y(E_x, \theta)$; discuss excitation of bound states and giant resonances; collective-model distorted-wave analysis.
Enriched target.

I. INTRODUCTION

For many years, inelastic scattering has been used to study low-lying collective excitations in nuclei. At energies above the Coulomb barrier, the multipolarity and strength of a transition in inelastic scattering are usually determined by fitting measured cross sections with predictions based on the distorted-wave Born approximation (DWBA). A useful measure of the total strength for all transitions of a given multipolarity is obtained by expressing the measured strength as a percentage depletion of a linearly energy-weighted sum rule (EWSR) limit.¹ One typically finds that for each multipolarity, only a small fraction of the EWSR strength is depleted by bound-state excitations.²

For each multipolarity, the strength not depleted by bound-state excitations should be located at higher excitation energies³ in the region of the nuclear continuum. If the expected EWSR strength is sufficiently localized in energy, one should then observe a giant resonance in inelastic scattering. A familiar example of a giant resonance in the nuclear continuum is the giant dipole ($E1$) resonance observed in photonuclear reactions. Since 1972, many experiments using inelastic scattering of electrons and nuclear projectiles have studied

collective excitations in the nuclear continuum.^{2,4} These studies have conclusively demonstrated the existence of a new giant resonance located 2–3 MeV lower in excitation energy than the giant dipole resonance. This resonance is most pronounced in nuclei with $A \geq 40$ and has a width of about 3–5 MeV.² The observed excitation energy of $E_x \approx 63A^{-1/3}$ MeV (Refs. 2 and 4) agrees with the prediction⁵ for an isoscalar giant quadrupole ($E2$) resonance.

The spin of the new resonance has usually been deduced by comparing measured cross-section angular distributions with DWBA predictions. Although early results could not distinguish between excitation of a quadrupole or a monopole ($E0$) resonance,⁴ later measurements using a variety of nuclear projectiles² have shown conclusively that most of the strength for the resonance results from an isoscalar $E2$ excitation. For $A \geq 40$, the observed $E2$ transition strength generally depletes at least half of the EWSR prediction.²

An alternative approach to resolving an ambiguity between $E2$ and $E0$ assignments for the new resonance was suggested by DWBA calculations⁶ which predicted that angular distributions of the *analyzing power*⁷ for incident *polarized* protons could distinguish between $L=2$ and $L=0$ excitations. In the present experiment, we have in-

vestigated this possibility by studying the $^{58}\text{Ni}(\vec{p}, p')$ reaction with a 60-MeV polarized proton beam. Some preliminary results were previously reported.⁸

The present experiment provides the first detailed investigation of polarization effects for inelastic excitations in the nuclear continuum. (Some proton polarization measurements have previously been reported.⁹) While our attempt to unambiguously identify the spin of the giant quadrupole resonance from the measured analyzing power was not successful,⁸ the measurements nonetheless provide an important new test of reaction theories describing the excitation of giant resonances. We have also obtained data for the giant dipole resonance, for a relatively weak resonance at $E_x = 13.5$ MeV ($\approx 53A^{-1/3}$ MeV), and for the unstructured nuclear continuum above the giant resonances. We have measured the cross section for the structure consisting of the giant quadrupole, giant dipole, and 13.5-MeV resonances in order to obtain the $E2$ EWSR strength in the giant resonance region of ^{58}Ni . The raw analyzing-power and cross-section data obtained from the polarized-beam spectra in the region of the nuclear continuum and the decomposition of the spectra into contributions from the resonances and the unstructured nuclear continuum are presented in Secs. VII and VIII. The results and analysis for the analyzing powers and cross sections for the resonances and the unstructured nuclear continuum are presented in Secs. IX and X.

In order to determine if the DWBA provides a satisfactory description of the analyzing power in proton inelastic scattering at 60 MeV, we have obtained data for low-lying bound states in ^{58}Ni having known J^π values. The analyzing power for bound states in ^{58}Ni and other fp -shell nuclei has previously been studied at energies between 18.6 and 40 MeV.¹⁰⁻¹⁴ Collective-model DWBA calculations give a good description of the analyzing powers only when a spin-orbit transition potential of the full-Thomas form is employed,¹⁵ particularly at the forwardmost angles where we have studied the analyzing power for the giant quadrupole resonance. A spin-orbit transition potential of the full-Thomas form has been employed in the present analyses. The results and analysis for the analyzing powers for low-lying bound states are presented in Secs. VI and X.

The spin-orbit term in the optical potential used in the present DWBA calculations is based on an optical-model analysis of elastic scattering analyzing power data at 30 and 40 MeV.¹⁶ We have tested the assumed spin-orbit potential at 60 MeV by measuring the analyzing power for elastic scattering from ^{58}Ni . The data are compared with the optical-model prediction in Sec. VI.

II. PRINCIPLE OF MEASUREMENTS WITH A POLARIZED PROTON BEAM

In this section, a brief outline of the principle of measurements of the analyzing power and the cross section with a polarized proton beam is given. The polarized beam was obtained from the atomic-beam polarized-ion source at the Oak Ridge isochronous cyclotron.¹⁷ Measurements were made at each scattering angle θ with spin-up and spin-down beams (polarization axis parallel and antiparallel to $\vec{k}_{\text{in}} \times \vec{k}_{\text{out}}$, respectively). The differential cross sections for spin up and spin down, $\sigma_+(\theta)$ and $\sigma_-(\theta)$, respectively, are given by

$$\sigma_{\pm}(\theta) = \sigma(\theta)[1 \pm p_{y\pm} A_y(\theta)], \quad (1)$$

where σ is the cross section for an unpolarized beam, and p_{y+} and p_{y-} are the beam polarizations for spin up and spin down. The quantity A_y , the analyzing power of the reaction, is equal to the polarization of the outgoing protons when the *inverse* reaction is initiated by unpolarized protons. The sign of the analyzing power is defined according to the Basel convention.¹⁸ From Eq. (1) the analyzing power is given by

$$A_y(\theta) = \frac{\sigma_+(\theta) - \sigma_-(\theta)}{p_{y+}\sigma_+(\theta) + p_{y-}\sigma_-(\theta)}. \quad (2)$$

If we introduce the mean beam polarization, $p_y \equiv \frac{1}{2}(p_{y+} + p_{y-})$, and the difference in beam polarization between spin up and spin down, $\delta \equiv \frac{1}{2}(p_{y+} - p_{y-})$, the cross section becomes

$$\sigma(\theta) = \frac{1}{2}[\sigma_+(\theta) + \sigma_-(\theta)] - (\delta/p_y)[\sigma_+(\theta) - \sigma_-(\theta)]. \quad (3)$$

Equation (2) shows that if δ is negligible, the analyzing power is directly proportional to the difference between the cross sections for spin up and spin down divided by their sum. Equation (3) shows that the cross section can be determined from polarized-beam measurements alone, and, if δ is negligible, is equal to the average of the cross sections for spin up and spin down.

III. EXPERIMENTAL METHOD

The analyzing power and the cross section for proton elastic and inelastic scattering from ^{58}Ni were measured at an incident energy of 60.2 ± 0.2 MeV. The ^{58}Ni target was a 99.95% enriched, 27.8-mg/cm² thick, self-supporting foil about 5 cm wide by 2 cm tall. At each angle, measurements were made with spin-up and spin-down beams having intensities typically 0.5–2 nA. The number of incident protons was determined by collecting the unscattered beam in a Faraday cup. Reaction protons were detected by nuclear emulsion plates placed in the focal plane of a broad-

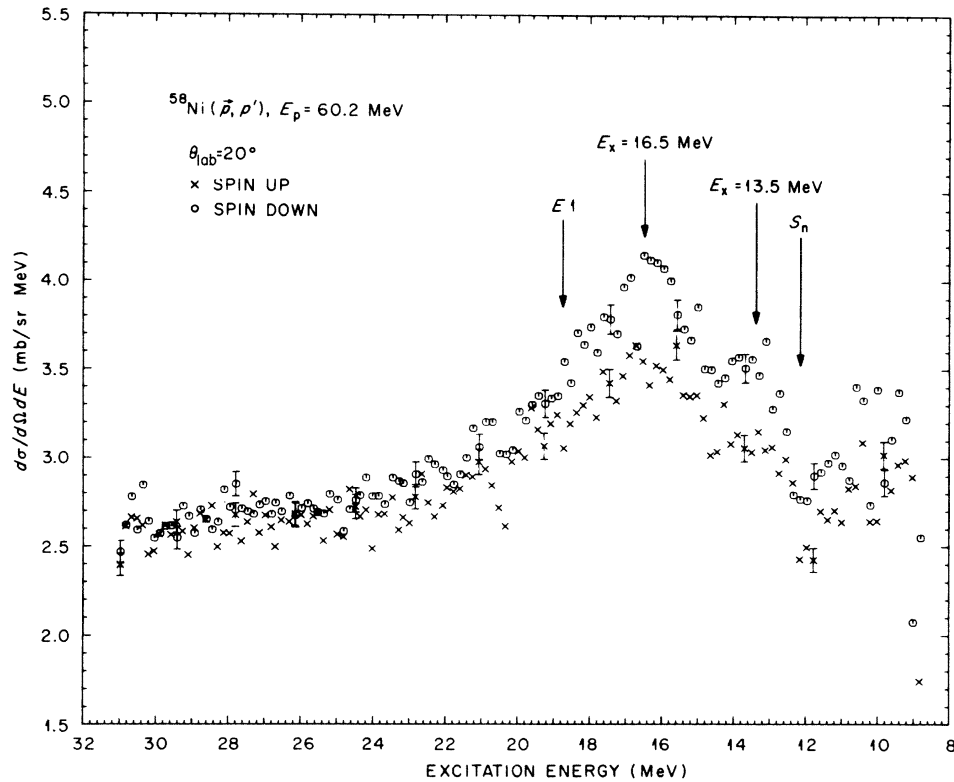


FIG. 1. Cross section vs excitation energy for incident spin-up and spin-down beams in the region of the nuclear continuum at $\theta_{1ab}=20^\circ$. S_n is the neutron separation energy and $E1$ is the known energy of the peak of the giant dipole resonance. The mean beam polarization for these data is $p_y=0.53$.

range magnetic spectrograph. The angular acceptance of the entrance aperture to the spectrograph was $\pm 1^\circ$. Absorber plates were placed in front of the emulsions to remove all reaction products other than protons.

The polarized-beam spectra were initially obtained at $\theta_{1ab}=15\text{--}40^\circ$ in 5° steps for the region $E_x \leq 31$ MeV. At a later time, polarized-beam spectra were obtained for the same energy region at $\theta_{1ab}=17.5\text{--}25^\circ$ in 2.5° steps, for the strongly excited bound states only at $\theta_{1ab}=15\text{--}60^\circ$ in 5° steps, and for elastic scattering at $\theta_{1ab}=15\text{--}65^\circ$ in 5° steps. Finally, an unpolarized beam was used to obtain spectra for the region $E_x \leq 31$ MeV at $\theta_{1ab}=12^\circ$ and $15\text{--}40^\circ$ in 5° steps. Equations (2) and (3) show that a comparison of the cross sections measured with polarized and unpolarized beams provides an important check on the absence of systematic errors in either of the two polarized-beam cross sections. Such errors can result in errors in the measured analyzing powers.

Polarized-beam spectra for the region $E_x \approx 9\text{--}31$ MeV at $\theta_{1ab}=20^\circ$ are shown in Fig. 1. The nuclear continuum lies above the neutron separation energy

($S_n = 12.2$ MeV¹⁹). In this region, the number of inelastically scattered protons was determined by scanning alternate $\frac{1}{2}\text{-mm} \times 2\text{-cm}$ bins on the nuclear emulsions. The track density was usually 250–550 per bin. Each data point in Fig. 1 was obtained by adding the number of tracks scanned in a 4-mm wide interval (≈ 160 keV) to obtain the statistical uncertainties of 2–3% shown with the data. On the basis of the observed positions of peaks of known excitation energy in the bound-state region, the uncertainty in excitation energy for the data points in the continuum region is estimated to be ± 0.2 MeV.

A polarized-beam spectrum for the bound-state region below $E_x = 5$ MeV at $\theta_{1ab} = 40^\circ$ is shown in Fig. 2. In this region, every $\frac{1}{2}\text{-mm} \times 2\text{-cm}$ bin on the nuclear emulsions was scanned. Track densities for strongly excited states were as large as 5000 per bin.

In order to obtain accurate cross sections in the region of the nuclear continuum, it is important that spurious background not contribute significantly to the spectra, since in many cases such background cannot be distinguished from genuine inelastic events.

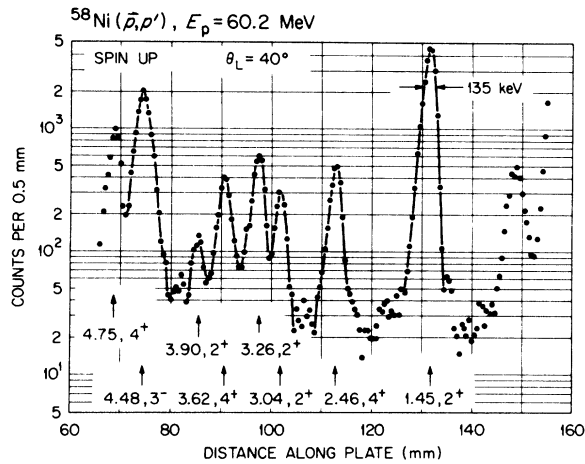


FIG. 2. Spectrum for incident spin-up beam in the bound-state region at $\theta_{\text{lab}} = 40^\circ$. The known excitation energies in MeV and J^π values are shown at the bottom of the figure.

Possible sources of unwanted background include the presence of lower-energy components in the incident beam and the scattering of the incident or scattered beam from objects such as slit edges and target frames into the spectrograph. Several procedures and tests were used throughout this experiment to insure that unwanted background was not present. The target frame, Faraday cup, and suppressor ring were constructed so that protons could not scatter from them into the entrance aperture of the spectrograph. The use of slits in the beam line was minimized. The optimum beam-focusing conditions were determined by beam transport calculations. These calculations were checked in a separate experiment by placing a scintillation counter behind the entrance slit of the spectrograph and measuring the spectrum of particles from ^{58}Ni and Pb targets at $\theta_{\text{lab}} = 6-20^\circ$. Finally, the ^{58}Ni data runs themselves were used to indicate the extent to which unwanted background was present. Comparison of spectra taken several months apart indicated no significant differences in the quality of the scattered beam dependent upon the time at which the data were taken. The small number of tracks in the bound-state region between the peaks below $E_x = 3$ MeV (see Fig. 2) indicated that a continuous low-energy tail from the elastic peak was not significant. The accuracy of the cross sections in the continuum region was checked by comparison with previous measurements on fp -shell nuclei at 62 MeV,²⁰ in which unwanted background was carefully minimized. All tests performed during the present experiment indicated that spurious background was not significant.

IV. MEASUREMENT OF THE BEAM POLARIZATION

The beam polarizations p_{y+} and p_{y-} were measured with a polarimeter employing proton elastic scattering from carbon (98.9% ^{12}C) at $\theta_{\text{lab}} = 60^\circ$. The target was a 1.1-mg/cm² thick polystyrene strip about 0.5 cm wide. The protons scattered to the left and right of the incident beam direction were detected in scintillation counters.

The polarimeter was located about 1 m in front of the spectrograph scattering chamber. Placing the polarimeter target in the beam had no observable effect on the spectrum of inelastically scattered protons in the spectrograph. For each data run, the beam polarization was determined by measuring the number of elastically scattered protons in the left (L) and right (R) detectors with polarized (+ or -) and unpolarized (u) beams. The beam polarizations are given by

$$p_{y\pm} = \pm \frac{1}{A_y(C)} \frac{r-1}{r+1}, \quad (4)$$

where r , the left-right asymmetry, is given by

$$r = \left(\frac{L}{R} \right)_+ \left(\frac{R}{L} \right)_u, \quad (5)$$

and $A_y(C)$ is the analyzing power for p -C scattering at $\theta_{\text{lab}} = 60^\circ$. The beam polarizations were typically $p_{y+} = 0.53-0.58$ and $p_{y-} = 0.55-0.60$.

The analyzing power of the polarimeter was measured in a separate experiment by comparing the left-right asymmetry at 60 MeV with the asymmetry at 49 MeV, where the analyzing power for p -C scattering is accurately known [$A_y(C) = +0.834 \pm 0.026$].²¹ The target for this measurement was a 49-mg/cm² thick carbon foil. The 60-MeV beam was degraded to 49 MeV by using an aluminum absorber. Successive runs with both polarized and unpolarized beams were made at the two energies. Simultaneous measurements at both energies were not required, since the beam polarization did not vary significantly with time. The analyzing power for p -C elastic scattering at 60 MeV and $\theta_{\text{lab}} = 60^\circ$ was determined to be $A_y(C) = +0.85 \pm 0.09$. The large uncertainty results mainly from the poor quality of the spectra at 49 MeV, where background from poor focusing of the energy-degraded beam was significant.

The uncertainty in the analyzing power of the polarimeter leads to an uncertainty of $\pm 10\%$ in the absolute normalization for all measured analyzing powers for $^{58}\text{Ni} + \bar{p}$ reactions. Additional uncertainties in the absolute normalization of the data are $\pm 3\%$ resulting from the uncertainty in the analyzing power for p -C scattering at 49 MeV (Ref. 21) and $\pm 1.5\%$ resulting from the uncertainty in the analyzing power for the polarimeter used

in Ref. 21. Uncertainties in absolute normalization are not shown with the data presented in Secs. VI, VII, and IX.

V. DWBA CALCULATIONS

In this paper, the measured analyzing powers and cross sections for inelastic excitation of giant resonances and bound states are compared with collective-model DWBA predictions (e.g., see Ref. 22). In all calculations, a complex transition potential with spin-orbit coupling was used and the effects of Coulomb excitation were included. The calculations used optical-model parameters given by Eqs. (3) and (5)–(7) of Ref. 16, except as noted.²³

The calculations for transitions with $L \geq 2$ were performed with the code DEFSP0.²⁴ This code incorporates a spin-orbit transition potential of the full-Thomas form.¹⁵ Calculations using the simplified Oak Ridge form of the spin-orbit transition potential¹⁰ were also performed with this code.

The predictions for $L=0$ and 1 excitations used in the present work are those previously calculated for the $^{60}\text{Ni}(\vec{p}, p')$ reaction at 61 MeV.^{6,25} The calculations employed a spin-orbit transition potential of the Oak Ridge form,¹⁰ which is identical to the full-Thomas form for $L=0$.⁶ The $L=1$ calculations in Ref. 25 incorrectly assumed destructive interference between Coulomb and nuclear excitation terms.²⁶ The calculations shown here used constructive interference between the two terms.

VI. ANALYZING POWERS FOR THE BOUND-STATE REGION

A. Analyzing power for elastic scattering

The measured analyzing power for proton elastic scattering from ^{58}Ni is shown in Fig. 3. The uncertainties in the data include statistics and an estimated uncertainty in the number of counts resulting from possible errors in scanning the nuclear emulsions. The latter uncertainty was $\pm 1-3\%$ for each spin direction depending upon the number of tracks in each scanning bin.

The curve in Fig. 3 is the optical-model prediction using the assumed parameters from Ref. 16 (see Sec. V). The predicted analyzing power gives reasonable agreement with the data, indicating that the assumed optical potential, particularly the spin-orbit term, should be adequate for the DWBA description of the analyzing powers for inelastic scattering at 60 MeV.

B. Analyzing powers for bound states

We have measured the analyzing powers for bound states in ^{58}Ni with $E_x(J^\pi) = 1.45(2^+)$, 2.46

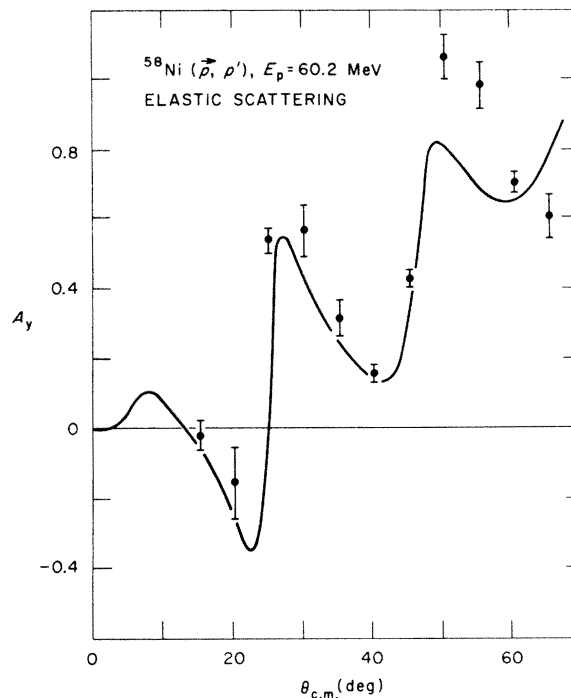


FIG. 3. Analyzing power for elastic scattering compared with an optical-model prediction using parameters from Ref. 16.

(4^+), 3.04 + 3.26 (2^+), 3.62 (4^+), 3.90 (2^+), 4.48 (3^-), and 4.75 (4^+) MeV.²⁷ For each polarized-beam spectrum (e.g., see Fig. 2), the total number of counts in each peak was determined and a background subtraction was performed based on the number of counts observed above and below the peak for the first 2^+ state. The analyzing powers are shown in Figs. 4 and 5. The uncertainties in the data include statistics, an estimated uncertainty in the subtracted background, and an estimated uncertainty of $\pm 1-3\%$ in the number of counts resulting from possible errors in scanning the nuclear emulsions. The curves shown in Figs. 4 and 5 are the DWBA predictions for the known multipolarity of each transition.

The DWBA is expected to be most applicable to the description of the analyzing powers for the strongly excited states at $E_x = 1.45$ and 4.48 MeV shown in Fig. 4.²² The calculations give a satisfactory qualitative description of the data for both states over the entire angular range studied. We note, however, that the data for $\theta_{\text{lab}} = 15-25^\circ$ tend to be more negative than the calculations. In Sec. IXA, we will show that these angles are of primary importance in the study of the analyzing power for the giant quadrupole resonance. The previous data at 40 MeV for strongly excited bound states in fp -shell nuclei¹⁰ have large uncertainties at the for-

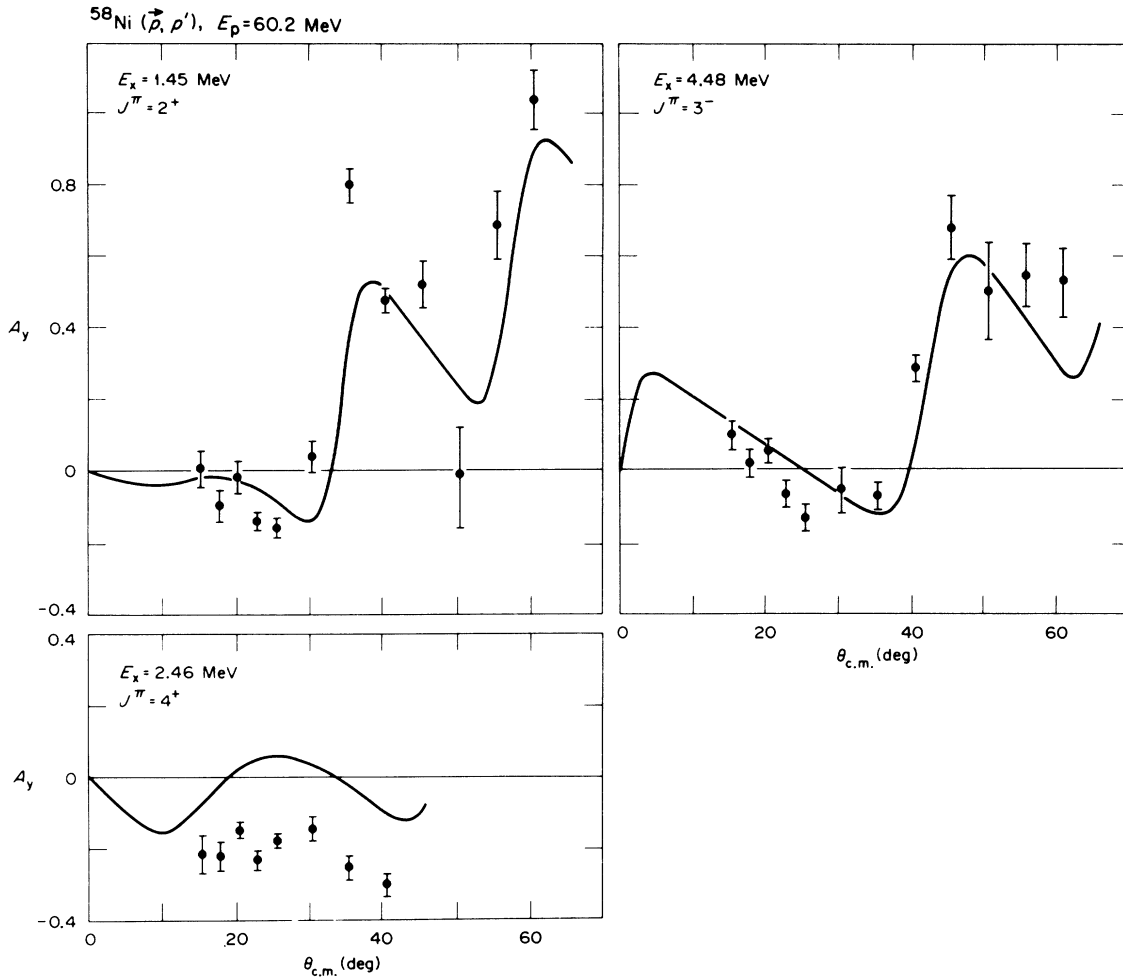


FIG. 4. Analyzing powers for strongly excited bound states compared with DWBA predictions.

wardmost angles, but an analysis¹⁵ similar to that presented here also shows a tendency for the forward-angle data to be more negative than the DWBA predictions.

The first 4^+ state at $E_x = 2.46$ MeV is also strongly excited, but it is not known if the DWBA should provide a valid description of the analyzing power since excitation via the intermediate first 2^+ state may also be important. We observe from Fig. 4 that the data are considerably more negative than the calculation at all angles.

Additional DWBA calculations for the strongly excited bound states with $J^\pi = 2^+$, 3^- , and 4^+ are presented in Sec. X.

The analyzing powers for the relatively weakly excited states are shown in Fig. 5. The 2^+ states at $E_x = 3.04$ and 3.26 MeV were treated as a single state, since they were not well resolved at all angles. The data for the 2^+ states at $E_x = 3.04 + 3.26$ MeV and the 4^+ states at $E_x = 3.62$ and 4.75

MeV are similar to the data for the strongly excited 2^+ and 4^+ states, respectively, shown in Fig. 4. Furthermore, the data for the weakly excited 2^+ and 4^+ states are more negative than the DWBA predictions, as was found in the analysis for the strongly excited states shown in Fig. 4. The data for the 2^+ state at $E_x = 3.90$ MeV bear little resemblance to the data for the other 2^+ states and to the DWBA predictions.

VII. ANALYZING POWERS AND CROSS SECTIONS IN THE CONTINUUM REGION

For each pair of polarized-beam spectra in the region of the nuclear continuum (e.g., see Fig. 1), the cross section and analyzing power at each excitation energy were calculated using Eqs. (2) and (3). Representative results at $\theta_{lab} = 20, 30,$ and 40° are shown in Fig. 6. The uncertainties in the data are statistical only. The uncertainty in the

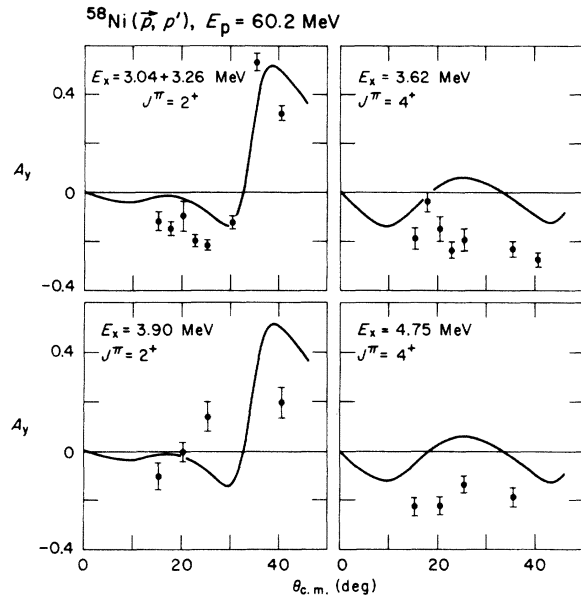


FIG. 5. Analyzing powers for weakly excited bound states compared with DWBA predictions.

absolute normalization of the cross sections resulting from uncertainties in target thickness, beam integration, and spectrograph solid angle is estimated to be $\pm 10\%$. One can show from Eq. (2) that these systematic uncertainties in the cross sections, which are presumably the same for both spin-up and spin-down beams, do not result in additional uncertainties in the analyzing powers. Checks to determine possible errors in scanning the nuclear emulsions in the continuum region showed that the number of tracks could be determined with an uncertainty of less than $\pm 1\%$. This uncertainty is negligible compared with the statistical uncertainties shown in Fig. 6.

The most prominent feature of the cross sections in the nuclear continuum is the giant quadrupole resonance centered at $E_x = 16.5 \pm 0.3$ MeV. The width of the resonance is about 4 MeV full width at half maximum (FWHM). The observed energy and width are in good agreement with other results from electron²⁸ and nuclear projectile²⁹⁻³¹ scattering. The giant dipole resonance centered at $E_x = 18.8$ MeV (Ref. 32) appears as a shoulder on the high excitation-energy side of the quadrupole resonance. [The excitation of the dipole res-

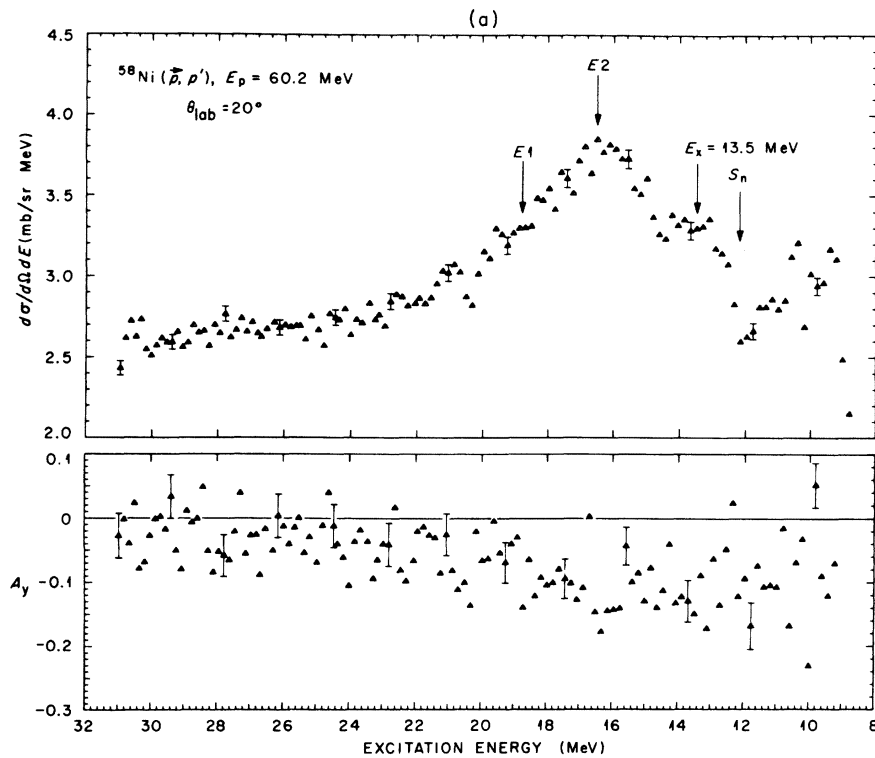


FIG. 6. Cross sections and analyzing powers vs. excitation energy in the region of the nuclear continuum at (a) $\theta_{lab} = 20^\circ$, (b) $\theta_{lab} = 30^\circ$, and (c) $\theta_{lab} = 40^\circ$. The neutron separation energy (S_n) and the energies of the giant quadrupole ($E2$), giant dipole ($E1$), and 13.5-MeV resonances are indicated.

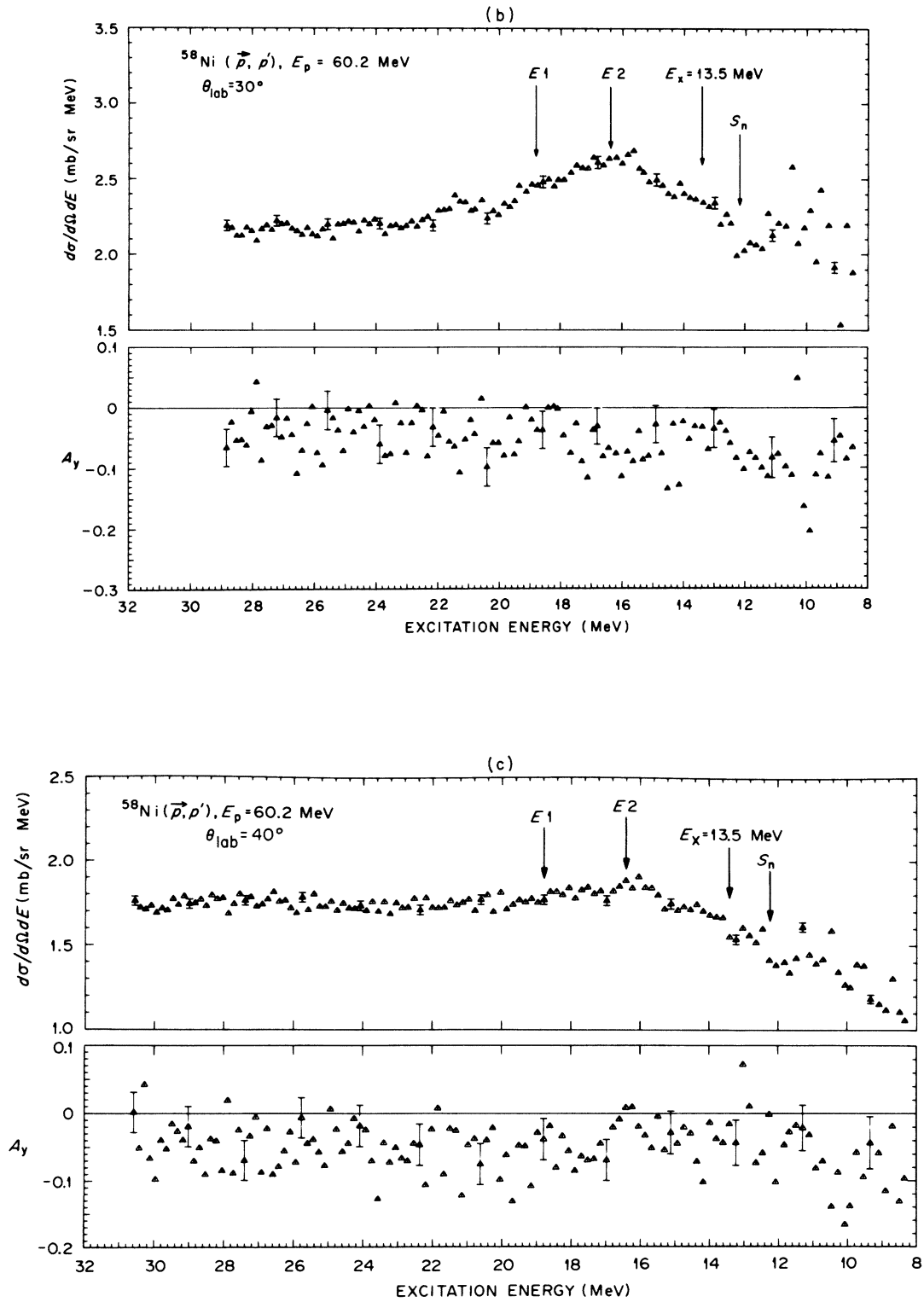


FIG. 6 (Continued)

onance in (p, p') is demonstrated more clearly in Ref. 30.] We observe a weaker resonance at $E_x \approx 13.5$ MeV with a width of about 2 MeV (FWHM). A resonance at this energy has been observed in electron^{28,33} and nuclear projectile^{29-31,34,35} scattering on fp -shell nuclei. In $^{58}\text{Ni}(e, e')$, the 13.5-MeV resonance appears as a doublet.²⁸ Previous spin assignments for the 13.5-MeV resonance are discussed in Sec. IX C.

A resonance at $E_x \approx 29$ MeV has been observed in the $^{58}\text{Ni}(e, e')$ reaction,²⁸ and was proposed as an isovector quadrupole ($E2$) excitation. No evidence for this resonance was found in the present work. However, an isovector quadrupole resonance is very difficult to observe at this excitation energy in (p, p') since the cross section is expected to be about an order of magnitude less than the cross section for the isoscalar quadrupole resonance at $E_x = 16.5$ MeV.

The analyzing powers in the nuclear continuum display two characteristic features. At all angles, the values in the region $E_x \approx 24$ –31 MeV above the

giant resonances are found to be small ($|A_y| < 0.1$ in most cases). On the other hand, the analyzing powers tend to be noticeably larger in the region $E_x \approx 12$ –20 MeV at those angles where the resonance structure is most pronounced.

VIII. DECOMPOSITION OF SPECTRA IN THE NUCLEAR CONTINUUM

The cross sections in the nuclear continuum presented in Fig. 6 show that the structure resulting from excitation of the giant resonances comprises only a small fraction of the inelastic cross section in the region $E_x \approx 12$ –24 MeV. Therefore, the extraction of resonance cross sections and analyzing powers from the data necessarily entails relatively large uncertainties. In this section, the methods used to decompose the spectra into contributions from the underlying continuum and the giant resonances are described. The decomposition of the spectra is illustrated in Fig. 7 for the cross sections at $\theta_{\text{lab}} = 20^\circ$.

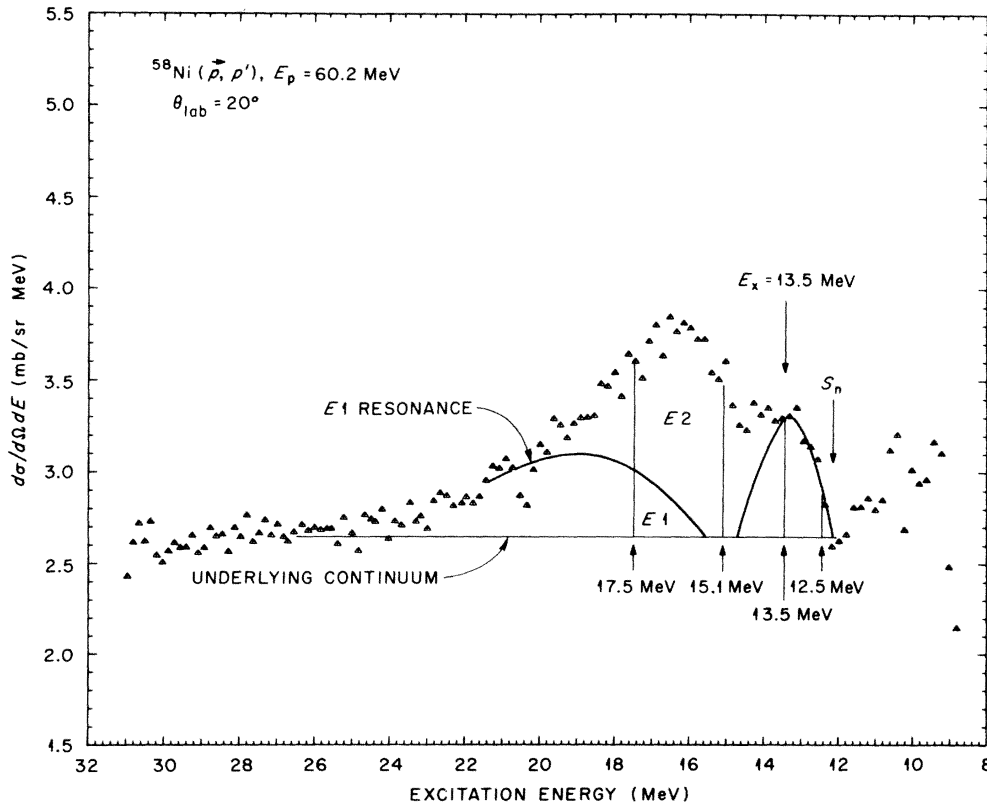


FIG. 7. Cross sections vs excitation energy in the region of the nuclear continuum at $\theta_{\text{lab}} = 20^\circ$. The assumed decomposition of the cross section (1) in the region $E_x = 15.1$ –17.5 MeV into contributions from the giant quadrupole ($E2$) and dipole ($E1$) resonances and the underlying continuum, and (2) in the region $E_x = 12.5$ –13.5 MeV into contributions from the 13.5-MeV resonance and the underlying continuum are shown (see Sec. VIII). S_n is the neutron separation energy.

The cross sections and analyzing powers obtained for the giant resonances depend critically upon the cross section and analyzing power assumed for the continuum underlying the resonances. The results in Fig. 6 illustrate that at each angle the cross section and analyzing power in the region $E_x \approx 24\text{--}31$ MeV above the giant resonances were found to be independent of excitation energy within statistical uncertainties. Furthermore, at the larger angles ($\theta_{\text{lab}} = 35$ and 40°) where the giant resonances are barely observable above the underlying continuum, the analyzing power for the entire continuum region $E_x \approx 12\text{--}31$ MeV was found to be independent of excitation energy within statistical uncertainties. Therefore, for each spin direction at each angle, we assumed that the cross-section contribution from the underlying continuum in the region of the giant resonances is given by a linear extrapolation of the constant cross section observed in the region $E_x \approx 25.5\text{--}31.0$ MeV. For all spectra, such an extrapolation joins smoothly either with the observed cross sections near the neutron separation energy for $\theta_{\text{lab}} = 15\text{--}30^\circ$ or, at $\theta_{\text{lab}} = 35$ and 40° where the 13.5-MeV resonance is not observable, with the observed cross sections below the quadrupole resonance near $E_x = 15$ MeV. Although our assumptions regarding the underlying continuum are reasonable and are consistent with all observed spectra, we emphasize that they cannot be rigorously verified either experimentally or by means of theoretical calculations.

The analyzing power and the relative cross section for the giant quadrupole resonance were obtained from the polarized-beam spectra in the region $E_x \approx 15.1\text{--}17.5$ MeV (see Fig. 7). This region was chosen in order to give a small contribution from the dipole resonance and avoid contributions from the 13.5-MeV resonance. The assumed cross-section contribution from the underlying continuum in this region varied from 69% for spin down at $\theta_{\text{lab}} = 20$ and 22.5° to 96% for spin down at $\theta_{\text{lab}} = 40^\circ$. The assumed contribution from the dipole resonance in this region is based on the resonance shape obtained from total photonuclear cross-section measurements on nickel³² (68.3% ^{58}Ni). We note that results from the $^{27}\text{Al}(n, p)^{27}\text{Mg}$ reaction³⁶ give good agreement between the dipole resonance shape in a direct reaction and the shape in photonuclear reactions. The $E1$ resonance shape was then normalized to the observed cross sections above the underlying continuum in the region $E_x \approx 21.0\text{--}24.0$ MeV, where the contribution from the quadrupole resonance is expected to be negligible.³⁰ The contribution from the dipole resonance to the total inelastic cross section in the region $E_x \approx 15.1\text{--}17.5$ MeV was less than 7% at all

angles.

The analyzing power and relative cross section for the 13.5-MeV resonance were obtained from the polarized-beam spectra in the region $E_x \approx 12.5\text{--}13.5$ MeV. This region was chosen to avoid contributions from the giant quadrupole resonance. The giant dipole resonance does not contribute significantly to the cross section in this region.

IX. RESULTS FOR GIANT RESONANCES AND THE UNDERLYING NUCLEAR CONTINUUM

A. Analyzing power for the giant quadrupole resonance

The analyzing power for the giant quadrupole resonance, obtained from the polarized-beam cross sections in the region $E_x \approx 15.1\text{--}17.5$ MeV, is shown in Fig. 8. (The relative cross section for the quadrupole resonance is discussed in Sec. IX C.) The data at $\theta_{\text{lab}} = 20$ and 25° are weighted averages of two separate measurements. The uncertainties in the data are statistical only and were obtained from the statistical uncertainties in the measured polarized-beam cross sections and in the assumed cross sections for the underlying continuum and the dipole resonance. Additional uncertainties resulting from errors in plate scanning and from the uncertainty in the shape of the dipole resonance³² were negligible.

An additional uncertainty in the analyzing power for the quadrupole resonance may arise from the possibility of a *systematic* error in the assumed cross sections for the underlying continuum in the region $E_x \approx 15.1\text{--}17.5$ MeV. If we assume that the analyzing power for the underlying continuum is independent of excitation energy, such a systematic error would be the same for both the spin-up and

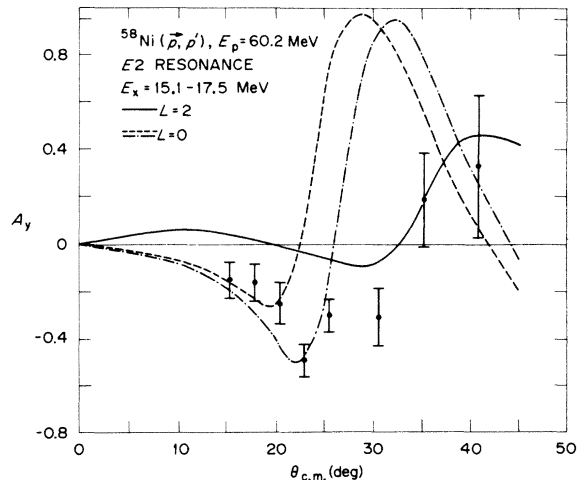


FIG. 8. Analyzing power for the giant quadrupole resonance compared with DWBA predictions. The two $L=0$ calculations are described in Sec. IX A.

spin-down cross sections. One can then show from Eq. (2) that the extracted analyzing power for the quadrupole resonance would be in error only when the analyzing powers for the quadrupole resonance and the underlying continuum are different. The most extreme case in our data occurs at $\theta_{lab} = 22.5^\circ$. At this angle, a systematic error of $\pm 5\%$ in the assumed polarized-beam cross sections for the underlying continuum would result in an error in the analyzing power for the quadrupole resonance of about ± 0.08 , which is larger than the statistical uncertainty of ± 0.067 . At $\theta_{lab} = 15^\circ$, where the analyzing power for the quadrupole resonance is the smallest, the same systematic error would result in an error in the analyzing power of about ± 0.03 , which is less than the statistical uncertainty of ± 0.076 . Uncertainties resulting from possible systematic errors in the assumed polarized-beam cross sections for the underlying continuum are not included in Fig. 8.

The curves shown in Fig. 8 are the DWBA predictions for $L=2$ and $L=0$ excitations. For an $L=0$ excitation, the dashed and dot-dashed curves are the predictions based on the transition potentials given by Eqs. (8) and (15) of Ref. 6, respectively.

Although it is known that the resonance at $E_x = 16.5$ MeV in ^{58}Ni is predominantly a quadrupole excitation,^{30,31} we find that the DWBA prediction for an $L=2$ excitation gives only a qualitative description of the angular dependence of the analyzing power. A marked discrepancy occurs for $\theta_{lab} = 15\text{--}30^\circ$, where the data are systematically more negative than the calculation. A similar effect was observed for the strongly excited, first 2^+ and 3^- bound states (see Sec. VIB and Fig. 4), but to a lesser extent than for the quadrupole resonance. The question of whether the $L=2$ calculation can provide more quantitative fits to the analyzing power for the quadrupole resonance by means of changes in the spin dependence of the transition potential or the optical-model parameters is examined in Sec. X.

The DWBA predictions for an $L=0$ excitation are found to give quantitative agreement with the data for $\theta_{lab} = 15\text{--}25^\circ$. However, the angular dependence of the data for $\theta_{lab} = 25\text{--}40^\circ$, particularly the negative analyzing power at $\theta_{lab} = 30^\circ$, bears no resemblance to the $L=0$ calculations. Therefore, we do not regard the agreement between the data and the $L=0$ calculations at the forwardmost angles as compelling evidence for a monopole excitation in the region $E_x = 15.1\text{--}17.5$ MeV. Further support for this conclusion is provided by the relative cross section in this region [see Sec. IX C and Fig. 10(a)].

Unfortunately, there are no known collective 0^+

bound states with which to test the $L=0$ DWBA predictions in the same way that the validity of $L=2$ calculations can be examined. A study of the $^{208}\text{Pb}(p, p')$ reaction at 45 MeV (Ref. 37) has identified an $E0$ resonance depleting about 7% of the EWSR strength. A measurement of the analyzing power for this resonance could provide an important test of the collective-model DWBA for $L=0$ excitations.

B. Analyzing power for the giant dipole resonance

The analyzing power for the giant dipole resonance, obtained from the polarized-beam cross sections in the region $E_x \approx 21.0\text{--}24.0$ MeV, is shown in Fig. 9. The uncertainties in the data are statistical only. The curves are the DWBA predictions for an $L=1$ excitation based on the Goldhaber-Teller and Jensen-Steinwedel models.²⁵ The measurements are not sufficiently precise to provide a meaningful test of the calculations. Although most of the data agree with the calculations, the data at most angles are also consistent with $A_y = 0$.

C. Cross section and analyzing power for the 13.5-MeV resonance

In previous electron scattering studies of the 13.5-MeV resonance in $f7p$ -shell nuclei, preliminary results for ^{56}Fe gave an $E3$ assignment,³³ but the results for a doublet in ^{58}Ni at $E_x = 13.2$

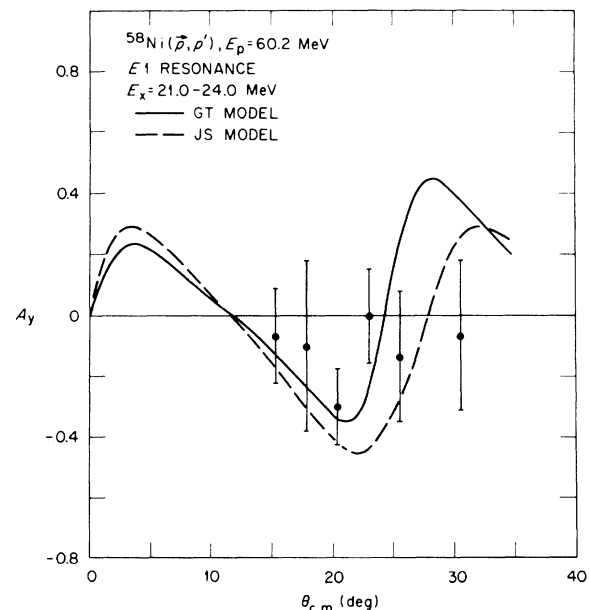


FIG. 9. Analyzing power for the giant dipole resonance compared with DWBA predictions based on Goldhaber-Teller (GT) and Jensen-Steinwedel (JS) models.

and 14.0 MeV gave $E2$ or $E0$ assignments.²⁸ A tentative $E3$ assignment was obtained from 155-MeV proton scattering on ^{56}Fe .³⁴ The most probable assignment from ^3He scattering on ^{56}Fe is $E2$, but an $E4$ assignment cannot be ruled out.³⁵ The cross sections observed in ^3He (Refs. 29 and 35) and α particle³¹ scattering appear to rule out an $E0$ assignment, since the $E0$ transition strength would far exceed the EWSR prediction.

The analyzing power and relative cross section for the 13.5-MeV resonance, obtained from the polarized-beam cross sections in the region $E_x \approx 12.5$ –13.5 MeV, are shown in Fig. 10. Also shown in Fig. 10(a) is the relative cross section for the giant quadrupole resonance, obtained from the data for the region $E_x \approx 15.1$ –17.5 MeV, normalized to the cross section for the 13.5-MeV resonance at $\theta_{\text{lab}} = 20^\circ$. The uncertainties in the cross sections and analyzing powers are statistical only. The curves are the DWBA predictions for $L=2$, $L=3$, and $L=0$ excitations; the calculated cross sections are normalized to the data at $\theta_{\text{lab}} = 20^\circ$. The $L=0$ curves are the calculations for the giant quadrupole resonance in ^{60}Ni at $E_p = 61$ MeV based on the transition potential given by Eq. (15) of Ref. 6.

From Fig. 10(a) we find that the cross section for the 13.5-MeV resonance is in reasonable agreement with both the data for the giant quadrupole resonance and the $L=2$ calculation, but is in poorer agreement with the $L=3$ calculation. The rise in the cross section at $\theta_{\text{lab}} = 12$ and 15° compared with the $L=2$ and $L=0$ calculations suggests that some monopole strength may also occur in the region of the 13.5-MeV resonance. However, more extensive measurements at angles forward of $\theta_{\text{lab}} = 15^\circ$ are needed to investigate this possibility.

The excellent agreement between the cross section for the giant quadrupole resonance and the $L=2$ calculation for $\theta_{\text{lab}} = 15$ – 35° provides additional evidence that most of the strength in the region $E_x \approx 15.1$ –17.5 MeV arises from an $E2$ rather than an $E0$ excitation. An analysis of the $^{58}\text{Ni}(d, d')$ reaction has shown that possible $L=0$ contributions to the cross section in the region of the giant quadrupole resonance comprise no more than $\approx 20\%$ of the $E0$ EWSR strength.³⁰ The rise in cross section at $\theta_{\text{lab}} = 12^\circ$ for the (p, p') reaction shown in Fig. 10(a), which may indicate an $L=0$ contribution, needs to be investigated by further measurements at forward angles.

The analyzing power for the 13.5-MeV resonance in Fig. 10(b) is similar to the data for the giant quadrupole resonance shown in Fig. 8. The agreement between the data and the $L=0$ prediction at most angles is probably fortuitous, since the analysis of the cross section in Fig. 10(a) in-

dicates that possible $L=0$ contributions are very small for $\theta_{\text{lab}} \geq 20^\circ$. The analyzing power cannot distinguish between $L=2$ and $L=3$ excitations, since the two DWBA predictions are similar.

In conclusion, our analysis of the cross section for the 13.5-MeV resonance agrees well with the result from ^3He scattering³⁵ that the resonance is predominantly an $E2$ excitation.

D. Cross section for the giant resonance structure

The cross section for the resonance structure in the region $E_x \approx 12.5$ –24.0 MeV is shown in Fig. 11. This region includes the giant quadrupole, giant dipole, and 13.5-MeV resonances. The estimated absolute uncertainties shown with the data are $\pm 20\%$ except $\pm 30\%$ at $\theta_{\text{lab}} = 35^\circ$. The uncertainties result mainly from the estimated absolute

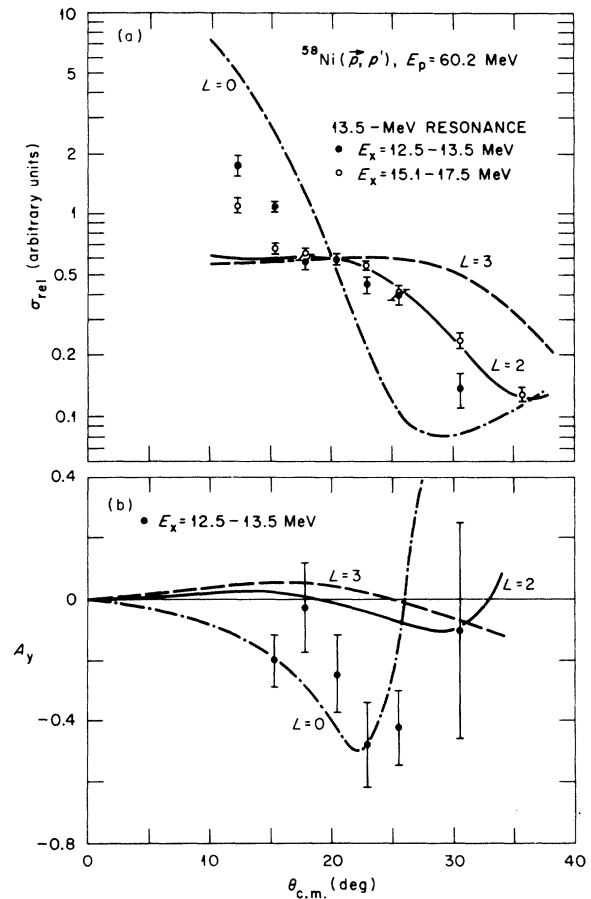


FIG. 10. (a) Relative cross sections for the 13.5-MeV and giant quadrupole resonances compared with DWBA predictions. The $L=0$ calculation is described in Sec. IX C. (b) Analyzing power for the 13.5-MeV resonance compared with DWBA predictions. The $L=0$ calculation is the same as the dot-dashed curve in Fig. 8.

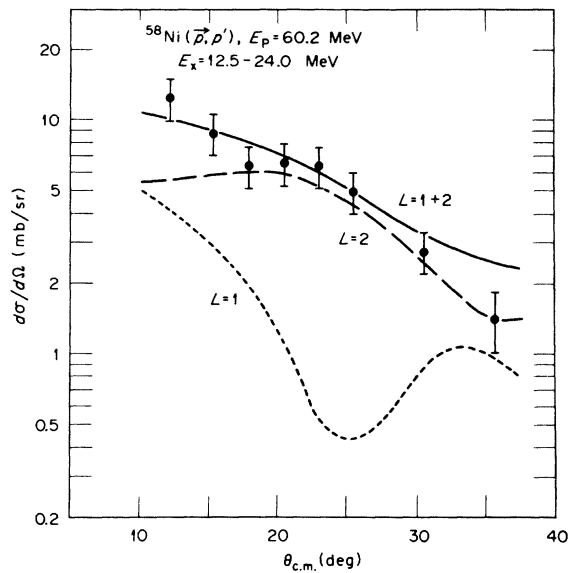


FIG. 11. Cross section for the structure comprising the giant quadrupole, giant dipole, and 13.5-MeV resonances compared with DWBA predictions for $L=1$ and $L=2$ excitations. The normalization of the calculations is described in Sec. IX D.

uncertainty in the measured cross sections in the continuum region (see Sec. VII) and the estimated uncertainty in the cross section for the underlying continuum. The cross section at $\theta_{lab} = 40^\circ$ could not be estimated with any reasonable degree of uncertainty.

The curves shown in Fig. 11 are the DWBA predictions for $L=1$ and $L=2$ excitations. The $L=1$ calculation is based on the Goldhaber-Teller model,²⁵ and is normalized to give 70% depletion of the EWSR strength in the region $E_x = 12.5$ – 24.0 MeV (see Fig. 26 of Ref. 32). The $L=2$ calculation is normalized to give 50% depletion of the EWSR strength, which is the value obtained from an analysis of the $^{58}\text{Ni}(d, d')$ reaction at 70 MeV.³⁰ The predicted cross section for the sum of the $L=1$ and $L=2$ excitations gives excellent agreement with the data.

E. Analyzing power for the unstructured nuclear continuum

From the measurements shown in Fig. 6, we found that the cross section and analyzing power in the region of the unstructured nuclear continuum above the giant resonances are independent of excitation energy within statistical uncertainties at all angles studied. At each angle, we have obtained the analyzing power for the region $E_x \approx 25.5$ – 31.0 MeV, and the results are shown in Fig. 12. The uncertainties include statistics and an additional $\pm 1\%$ uncertainty in the number of

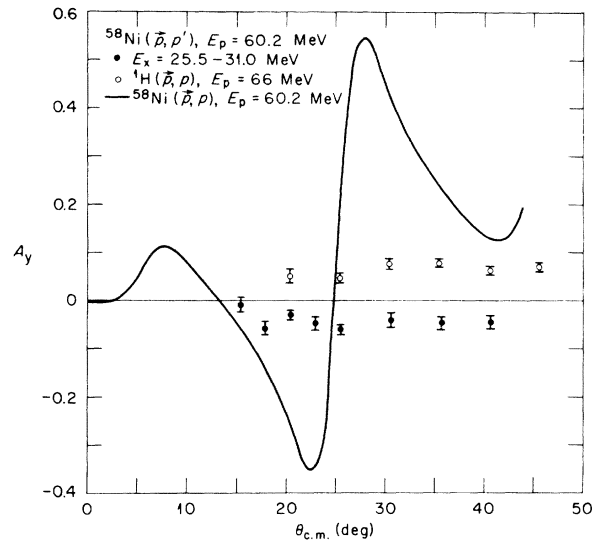


FIG. 12. Analyzing power in the region of the unstructured nuclear continuum compared with the analyzing power for proton elastic scattering from ^1H at $E_p = 66$ MeV and an optical-model prediction for the analyzing power for proton elastic scattering from ^{58}Ni at $E_p = 60.2$ MeV. The comparisons are described in Sec. IX E.

counts for each spin direction to account for possible errors in plate scanning.

Although the analyzing power for the unstructured nuclear continuum is small, the values are nonzero over most of the angular range studied. It is possible that the analyzing power results in part from a continuous background in the spectra (see Sec. III). One possible source of an unstructured background is a low-energy tail from the elastic scattering peak. If such background were significant, the analyzing power for the nuclear continuum should be similar in shape to the analyzing power for elastic scattering. The curve in Fig. 12 is the optical-model prediction for elastic scattering shown in Fig. 3. While the elastic scattering analyzing power shows strong oscillations, the data for the nuclear continuum are essentially independent of angle. Therefore, the analyzing power most likely does not result from background from elastic scattering.

The intranuclear cascade model has recently been applied to a study of inelastic proton spectra in the nuclear continuum at $E_p = 62$ MeV.³⁸ In this model, the inelastic scattering process is described by a sequence of nucleon-nucleon collisions within the target nucleus. At the angles and excitation energies for the data shown in Fig. 12, the model predicts that most of the inelastically scattered protons result from a single collision with a target nucleon.^{20,38} Therefore, the measured analyzing power in the nuclear continuum

might be expected to resemble measurements for free nucleon-nucleon scattering. Shown in Fig. 12 is the analyzing power for the $^1\text{H}(\bar{p}, p)$ reaction at 66 MeV.³⁹ The data for proton-proton scattering show essentially the same angular dependence and have about the same magnitude as the data for the nuclear continuum, but the two sets of data are opposite in sign. The qualitative similarities between the analyzing powers for the nuclear continuum and proton-proton scattering perhaps provide encouraging support for the intranuclear cascade model. Therefore, it would be interesting to include spin-dependent effects in the calculations and attempt to reproduce our measurements.

Another possible source of the nonzero analyzing powers in the unstructured nuclear continuum is a significant cross-section contribution from one-step collective excitation processes, since our measurements for the giant resonances show that such excitations can have large analyzing powers. If collective excitations are present in the region $E_x = 25.5\text{--}31.0$ MeV, the resonances are either too weak or too broad to be observed as structure in the cross section.

X. FURTHER ANALYSIS OF THE ANALYZING POWERS FOR THE GIANT QUADRUPOLE RESONANCE AND BOUND STATES

In Secs. VIB and IXA, the measured analyzing powers for strongly excited bound states and the giant quadrupole resonance were found to be consistently more negative than the DWBA calculations at $\theta_{\text{lab}} = 15\text{--}30^\circ$, although the calculations give a qualitative description of the data over the entire angular range studied. In this section, we investigate the possibility that improved fits to the inelastic analyzing powers at forward angles can be obtained by varying either the spin-orbit transition potential or the optical-model parameters. Additional calculations are compared with the data for the giant quadrupole resonance and the strongly excited bound states at E_x (J^π) = 1.45 (2^+), 2.46 (4^+), and 4.48 (3^-) MeV.

A. Effect of changes in the spin-orbit transition potential

In Fig. 13, the DWBA calculations employing a spin-orbit transition potential of the full-Thomas form¹⁵ are compared with calculations employing the simplified Oak Ridge form¹⁰ and calculations with no spin-orbit transition potential. Also shown are calculations using the full-Thomas form in which the spin-orbit deformation β_{so} is larger than the central deformation β_0 (e.g., see Refs. 15 and 22).

The calculations using the full-Thomas form give significantly better fits to the forward-angle data than the calculations using the Oak Ridge form, particularly for the two $L=2$ transitions. Similar results were previously obtained at 40 MeV.¹⁵ Somewhat surprisingly, the calculations for the $L=2$ transitions with no spin-orbit transition potential give a better description of some of the forward-angle data than the calculations using the full-Thomas form. However, the calculations with no spin-orbit transition potential give a considerably greater variation of the analyzing power with angle forward of $\theta_{\text{lab}} = 40^\circ$ than is shown by the data. When the full-Thomas form is used, the calculations with $\beta_{\text{so}} = 1.5\beta_0$ give slightly better fits to the data than the calculations with $\beta_{\text{so}} = \beta_0$, in agreement with a previous analysis at 40 MeV.¹⁵ However, the uncertainties in the data and the quality of the fits are not sufficient to give a clear preference between the two values for the spin-orbit deformation.

B. Effect of changes in optical-model parameters

All calculations presented in this section employed a spin-orbit transition potential of the full-Thomas form and equal spin-orbit and central deformation parameters.

The results shown in Fig. 14 investigate the effects on the DWBA calculations of increasing a_w from 0.293 to 0.54 fm or decreasing a_{so} from 0.738 to 0.5 fm. These parameter variations produce only small changes in the predicted elastic scattering analyzing power for $\theta_{\text{lab}} < 90^\circ$. Increasing a_w has an insignificant effect on the DWBA calculations. However, decreasing a_{so} results in significant improvements in the fits for all transitions at $\theta_{\text{lab}} = 15\text{--}40^\circ$, without affecting the quality of the fits at larger angles. This analysis suggests that the inelastic analyzing power may be considerably more sensitive to the geometry of the spin-orbit potential than is elastic scattering.

The optical potential used in the present analysis contains a real spin-orbit term only. Some previous analyses of inelastic scattering analyzing powers, mostly at 155–185 MeV, included in addition an imaginary spin-orbit term in the optical potential.^{11,40-43} In these analyses, a *repulsive* potential (i.e., opposite in sign to the real spin-orbit potential) of depth $W_{\text{so}} \approx -0.1$ to -3.2 MeV was used. At energies above about 100 MeV where the impulse approximation is expected to be valid,⁴⁴ it has been shown that one expects $W_{\text{so}} \approx -1$ MeV.⁴⁵ The results in Fig. 15 show the effects on the DWBA calculations of adding an imaginary spin-orbit term to the optical potential with $W_{\text{so}} = \pm 2$ MeV. We find that the addition of an *at-*

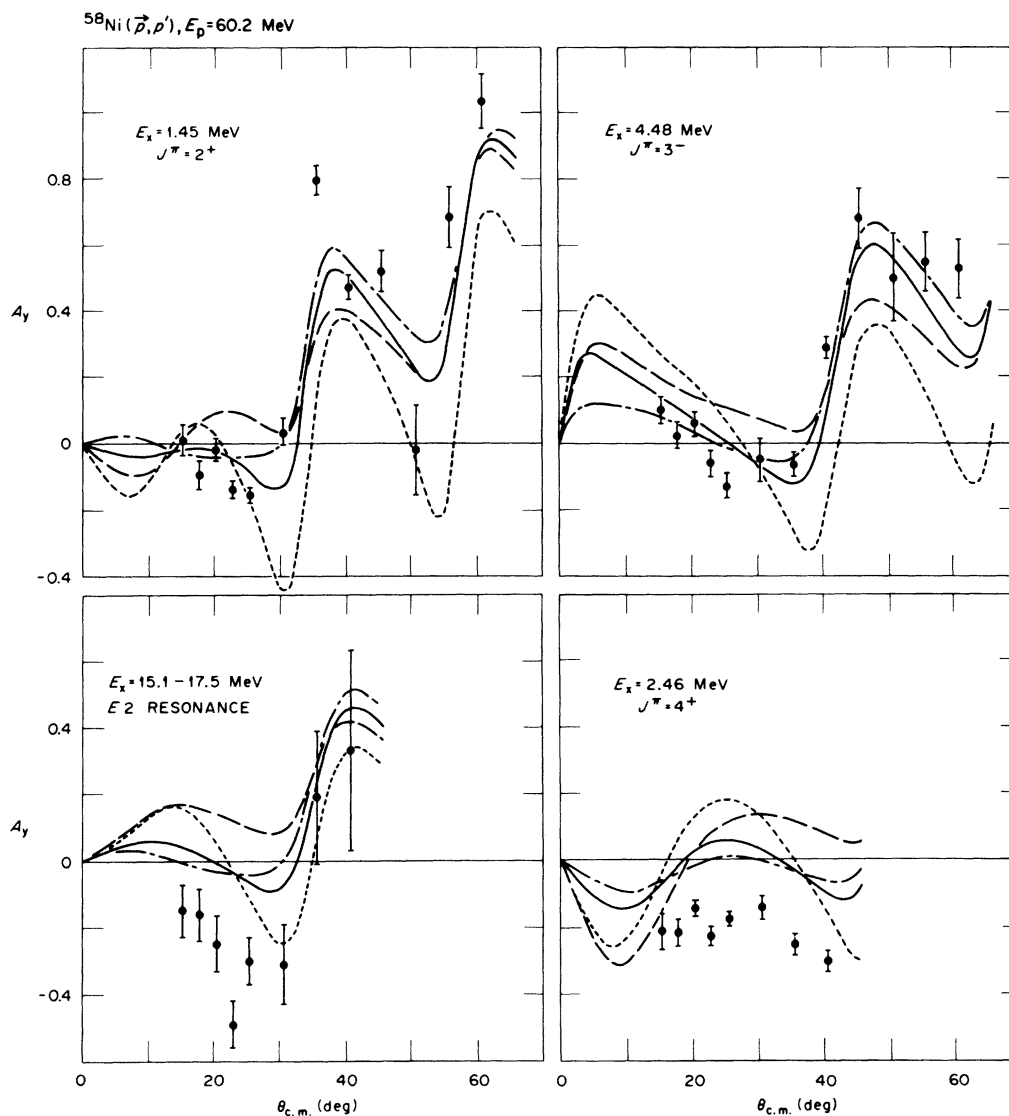


FIG. 13. Analyzing powers for the giant quadrupole resonance and strongly excited bound states compared with DWBA predictions employing a spin-orbit transition potential of the full-Thomas form (solid curves), the simplified Oak Ridge form (long-dashed curves), no spin-orbit transition potential (short-dashed curves), and the full-Thomas form with $\beta_{so} = 1.5\beta_0$ (dot-dashed curves).

tractive imaginary spin-orbit term produces significantly more negative analyzing powers at forward angles resulting in better agreement with the data for all transitions, particularly for the giant quadrupole resonance. We note that the additional spin-orbit term also produces significant changes in the predicted elastic scattering analyzing power at all angles. Therefore, it might be more meaningful to introduce the imaginary spin-orbit term, adjust the other optical-model parameters to fit the elastic data, and then perform the inelastic scattering calculations. Nonetheless, our analysis provides the first evidence that an

attractive imaginary spin-orbit potential might be applicable to the description of inelastic scattering analyzing powers at energies less than those where the impulse approximation is normally used and a repulsive spin-orbit potential is appropriate.

In Fig. 16, the DWBA calculations using the optical-model parameters from Ref. 16 are compared with calculations using two different parameter sets—one based on an analysis of the $^{58}\text{Ni}(\vec{p}, p)$ reaction at 40 MeV,⁴⁶ and the other based on (\vec{p}, p) data for $A > 40$ and $E_p < 50$ MeV.⁴⁷ The calculations using the parameters from Ref. 47 are not significantly different from those using the parameters

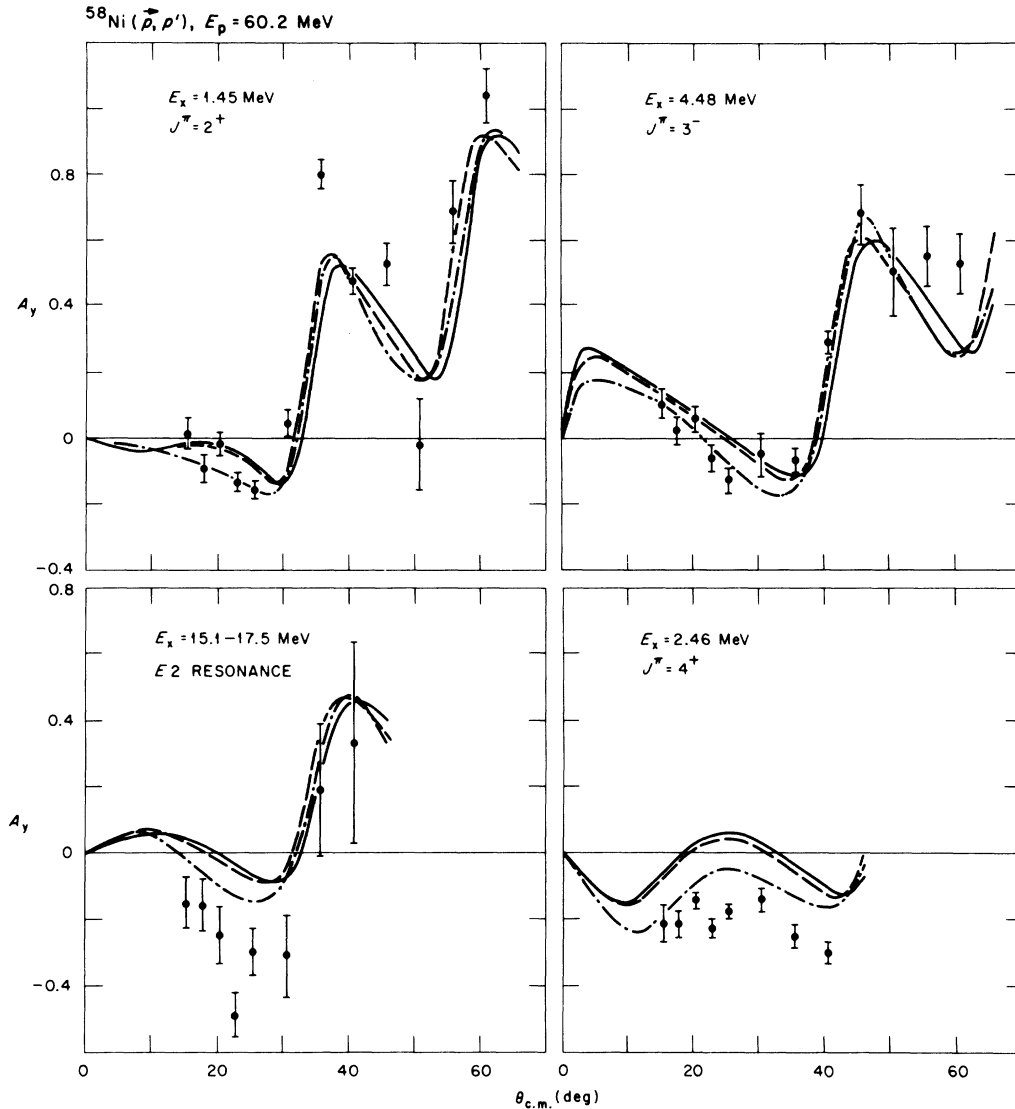


FIG. 14. Analyzing powers for the giant quadrupole resonance and strongly excited bound states compared with DWBA predictions using the optical-model parameters of Sec. V (solid curves), the same parameters with $a_w = 0.54$ fm instead of 0.293 fm (dashed curves), and the same parameters with $a_{so} = 0.5$ fm instead of 0.738 fm (dot-dashed curves).

from Ref. 16. Using the parameters from Ref. 46 gives some improvement in the fits to the forward-angle data for the quadrupole resonance and the 3^- and 4^+ bound states, but the fits at the larger angles are poorer for the 2^+ and 3^- bound states. We note that the parameters from Ref. 47 give a good fit to the elastic scattering analyzing power, but the parameters from Ref. 46 give a significantly poorer fit to the data.

The distorted-wave code DEFSP0²⁴ requires that the same optical-model parameters be used for the incoming and outgoing channels. However, several of the parameters from Ref. 16 are energy dependent. Therefore, it might be more ap-

propriate to perform the calculations for the giant quadrupole resonance with the proper parameters for both channels, since the excitation energy is large (16.5 MeV). We note that a calculation using parameters for $E_p = 43.7$ MeV gives analyzing powers at $\theta_{lab} = 15-25^\circ$ which are 0.04-0.05 more negative than the calculation for $E_p = 60.2$ MeV shown in Fig. 8, thus giving better agreement with the data.

XI. SUMMARY AND CONCLUSIONS

This paper has presented a study of the $^{58}\text{Ni}(\vec{p}, p')$ reaction at 60 MeV. This experiment provides for the first time a detailed study of the analyzing

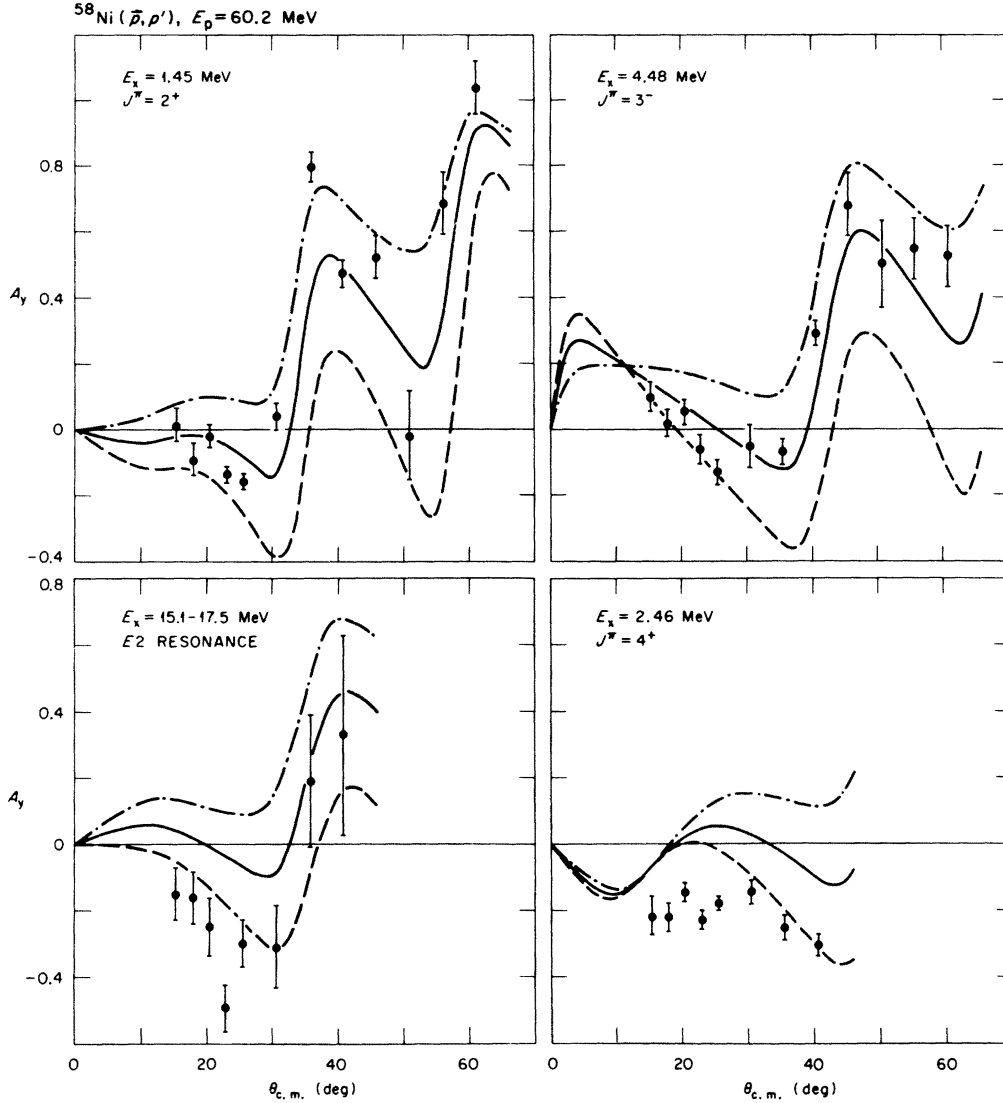


FIG. 15. Analyzing powers for the giant quadrupole resonance and strongly excited bound states compared with DWBA predictions using the optical-model parameters of Sec. V (solid curves), the same parameters with an attractive imaginary spin-orbit term with $W_{so} = +2$ MeV (dashed curves), and the same parameters with a repulsive imaginary spin-orbit term with $W_{so} = -2$ MeV (dot-dashed curves).

power in the region of the nuclear continuum. The analyzing powers for several bound states below $E_x = 5$ MeV were also studied. The measurements for giant resonances and bound states were compared with collective-model DWBA calculations employing a spin-orbit transition potential of the full-Thomas form and optical-model parameters which give a good description of the measured elastic scattering analyzing power at 60 MeV.

The measured analyzing power for the isoscalar giant quadrupole resonance at $E_x = 16.5$ MeV ($\approx 63A^{-1/3}$ MeV) was found to be systematically more negative than the DWBA prediction for an

$L = 2$ excitation at $\theta_{lab} = 15-30^\circ$, although the prediction gave a qualitative description of the data over the entire angular range studied ($\theta_{lab} = 15-40^\circ$). The marked discrepancy between the data and the calculation at the forwardmost angles was somewhat unexpected, since the DWBA calculations gave better fits to the data at $\theta_{lab} = 15-30^\circ$ for the strongly excited 2^+ and 3^- bound states. The fits to the data for the more weakly excited bound states were poorer than for the strongly excited 2^+ and 3^- states, but processes other than the single-step excitation mechanism described by the DWBA may be important for weak transi-

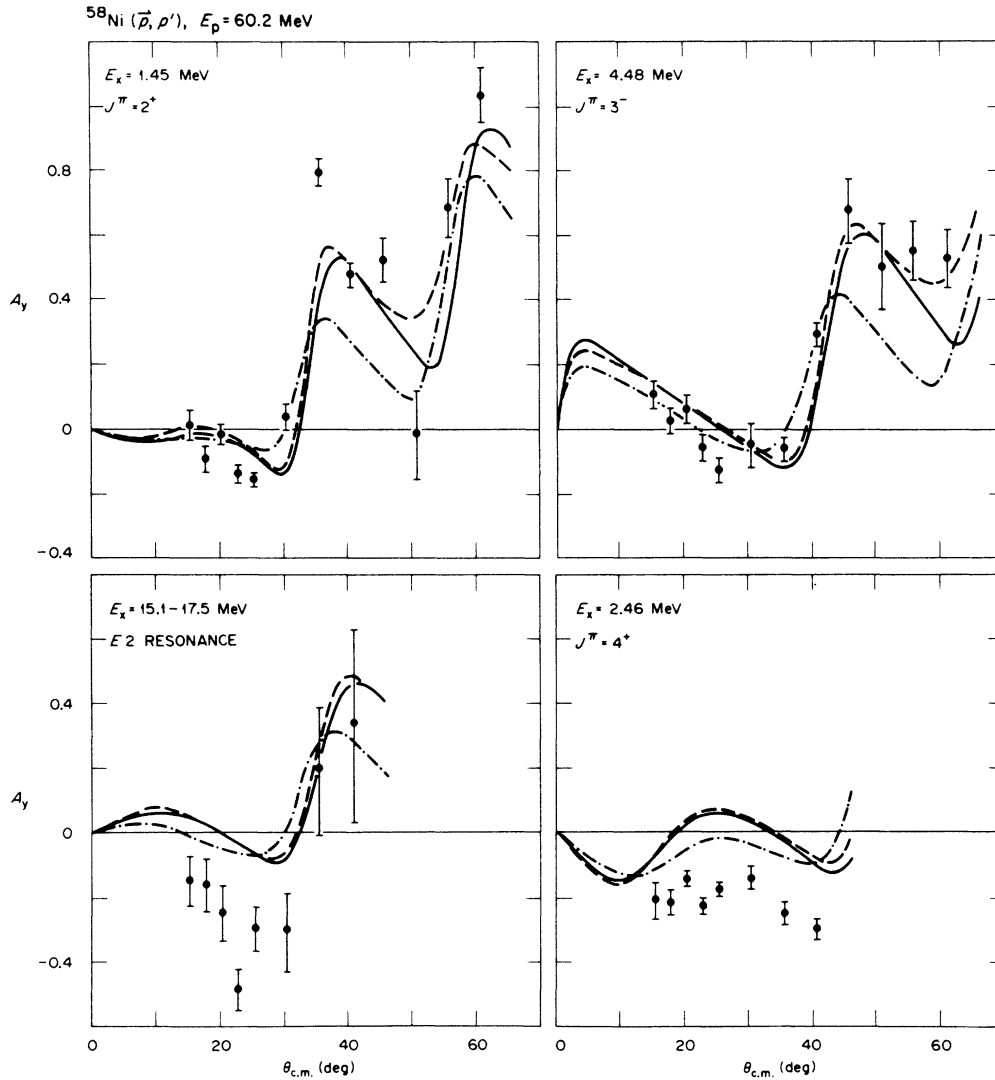


FIG. 16. Analyzing powers for the giant quadrupole resonance and strongly excited bound states compared with DWBA predictions using the optical-model parameters of Sec. V (solid curves), optical-model parameters from Ref. 47 (dashed curves), and optical-model parameters from Ref. 46 (dot-dashed curves).

tions. Complex excitation mechanisms are probably not responsible for the discrepancy between theory and experiment for the giant quadrupole resonance, since the resonance depletes about 50% of the isoscalar $E2$ EWSR strength. In our analysis, significant improvements in the fits to the analyzing power for the giant quadrupole resonance were obtained by decreasing the spin-orbit diffuseness parameter or by adding an attractive imaginary spin-orbit term to the optical potential.

The discrepancy between the measured analyzing power for the giant quadrupole resonance and the collective-model DWBA prediction for an $L=2$ excitation will hopefully stimulate further experimental work. For experiments with po-

larized protons, available cross-section measurements² indicate that the quadrupole resonance is most easily observed above the underlying continuum if medium-weight nuclei ($A \approx 40-120$) are used and if the bombarding energy is increased to at least 150 MeV. Another interesting possibility for studying spin-dependent effects in the excitation of the giant quadrupole resonance is to use incident polarized deuterons. Compared with protons, deuterons offer the advantages that the cross section for the quadrupole resonance is significantly enhanced relative to the underlying continuum and that the giant dipole resonance is not excited to a significant degree.³⁰

Further theoretical investigations of the ana-

lyzing powers for the bound states and the giant quadrupole resonance might shed light on the nature of the spin-orbit interaction in nucleon-nucleus scattering. The spin-orbit transition potential of the full-Thomas form used in the present analysis is essentially a phenomenological potential, although the same form can be derived in the impulse approximation.⁴⁸ The full-Thomas form does not include spin-spin or tensor terms in the nucleon-nucleus interaction. The impulse approximation, which can include these terms in the effective nucleon-nucleon interaction, has been successfully applied to the analysis of inelastic scattering analyzing powers at energies above 150 MeV.^{40, 43, 49} It would be interesting to investigate the effects of the additional spin-dependent interactions on the present calculations.

Most analyses of cross sections and analyzing powers for bound states and the giant quadrupole resonance have employed the macroscopic collective-model DWBA used in the present analysis. Recently, microscopic-model DWBA calculations for the excitation of giant resonances have been performed for some doubly magic nuclei.^{2, 4} Microscopic-model analyses are important because they yield specific predictions concerning the excitation energies, multipolarities, and transition strengths of the components of the giant resonance structure. The macroscopic collective model,

on the other hand, does not incorporate specific nuclear structure information in the theory. The microscopic-model analyses performed so far have been relatively crude, in that the imaginary part of the effective nucleon-nucleon interaction is not well known and the spin dependence of the interaction is usually neglected.⁵⁰ Nonetheless, calculations have shown considerable success in fitting cross sections in the giant resonance region.⁵⁰⁻⁵³ A microscopic-model analysis of the analyzing powers and cross sections in the nuclear continuum measured in the present experiment could yield important information on the multipole composition of the giant resonance region of ⁵⁸Ni and on the nature of the effective nucleon-nucleon interaction describing the scattering process.

XII. ACKNOWLEDGMENTS

The authors are indebted to R. S. Lord, M. L. Mallory, and S. W. Mosko and to the Oak Ridge isochronous cyclotron operations staff for their tireless efforts in operating the polarized-ion source and the cyclotron. The authors are also grateful to V. Jones and R. Shelton for their rapid and efficient completion of the monumental task of scanning the more than 42 m of plates exposed during this experiment.

*Research sponsored by the U. S. Energy Research and Development Administration under contract with Union Carbide Corporation.

¹A. M. Lane, *Nuclear Theory* (Benjamin, New York, 1964).

²F. E. Bertrand, *Annu. Rev. Nucl. Sci.* (to be published) and references therein.

³O. Nathan and S. G. Nilsson, in *Alpha-, Beta- and Gamma-Ray Spectroscopy*, edited by K. Siegbahn (North-Holland, Amsterdam, 1965), Vol. 1, p. 601.

⁴G. R. Satchler, *Phys. Rep.* **14C**, 97 (1974), and references therein.

⁵A. Bohr and B. R. Mottelson, *Nuclear Structure*, (Benjamin, New York, 1975) Vol. II.

⁶G. R. Satchler, *Part. Nucl.* **5**, 105 (1973).

⁷*Polarization Phenomena in Nuclear Reactions*, edited by H. H. Barschall and W. Haerberli (The University of Wisconsin Press, Madison, Wisconsin, 1971), p. xxv.

⁸D. C. Kocher, F. E. Bertrand, E. E. Gross, R. S. Lord, and E. Newman, *Phys. Rev. Lett.* **31**, 1070 (1973); **32**, (E)264(1974); F. E. Bertrand, E. E. Gross, D. C. Kocher, and E. Newman, in *Proceedings of the International Conference on Nuclear Structure and Spectroscopy, Amsterdam, 1974*, edited by H. P. Blok and A. E. L. Dieperink (Scholar's Press, Amsterdam, 1974), Vol. I, p. 165; D. C. Kocher, F. E. Bertrand, E. E. Gross, and E. Newman, ORNL Report No. ORNL-5025,

1975 (unpublished), p. 61.

⁹A. Johansson, G. Tibell, and P. Hillman, *Nucl. Phys.* **11**, 540 (1959).

¹⁰M. P. Fricke, E. E. Gross, and A. Zucker, *Phys. Rev.* **163**, 1153 (1967).

¹¹C. Glashauser, R. de Swinarski, J. Thirion, and A. D. Hill, *Phys. Rev.* **164**, 1437 (1967).

¹²D. J. Baugh, M. J. Kenny, J. Lowe, D. L. Watson, and H. Wojciechowski, *Nucl. Phys.* **A99**, 203 (1967).

¹³O. Karban, P. D. Greaves, V. Hnizdo, J. Lowe, and G. W. Greenlees, *Nucl. Phys.* **A147**, 461 (1970).

¹⁴P. D. Greaves, V. Hnizdo, J. Lowe, and O. Karban, *Nucl. Phys.* **A179**, 1 (1972).

¹⁵H. Sherif, *Nucl. Phys.* **A131**, 532 (1969).

¹⁶J. J. H. Menet, E. E. Gross, J. J. Malanify, and A. Zucker, *Phys. Rev. C* **4**, 1114 (1971).

¹⁷ORNL Reports No. ORNL-4217, 1968 (unpublished), p. 106; No. ORNL-4404, 1969 (unpublished), p. 96; No. ORNL-4534, 1970 (unpublished), p. 75; and No. ORNL-4649, 1971 (unpublished), p. 99.

¹⁸*Proceedings of the International Conference on Polarization Phenomena of Nucleons, Basel, Switzerland, 1960*, edited by P. Huber and K. P. Meyer (Helv. Phys. Acta Suppl. VI, 1961), p. 436.

¹⁹A. H. Wapstra and N. B. Gove, *Nucl. Data* **A9**, 303 (1971).

²⁰F. E. Bertrand and R. W. Peelle, *Phys. Rev. C* **8**, 1045

- (1973), and references therein.
- ²¹R. M. Craig, J. C. Dore, G. W. Greenlees, J. Lowe, and D. L. Watson, Nucl. Phys. 83, 493 (1966).
- ²²G. R. Satchler, in *Polarization Phenomena in Nuclear Reactions*, edited by H. H. Barschall and W. Haeblerli (The University of Wisconsin Press, Madison, Wisconsin, 1971), p. 155.
- ²³The value $a_{90} = 0.78$ fm in Ref. 16 should be 0.738 fm.
- ²⁴W. Van Rij (private communication).
- ²⁵G. R. Satchler, Nucl. Phys. A195, 1 (1972).
- ²⁶G. R. Satchler, Nucl. Phys. A224, 596(E) (1974).
- ²⁷S. Raman, Nucl. Data B3(3,4), 145 (1970).
- ²⁸Y. Torizuka, Y. Kojima, T. Saito, K. Itoh, and A. Nakada, Research Report of the Laboratory of Nuclear Science, Tohoku University, 1973 (unpublished), Vol. 6, p. 165.
- ²⁹A. Moalem, W. Benenson, and G. M. Crawley, Phys. Rev. Lett. 31, 482 (1973).
- ³⁰C. C. Chang, F. E. Bertrand, and D. C. Kocher, Phys. Rev. Lett. 34, 221 (1975).
- ³¹D. H. Youngblood, J. M. Moss, C. M. Rozsa, J. D. Bronson, A. D. Bacher, and D. R. Brown, Phys. Rev. C 13, 994 (1976).
- ³²J. M. Wycoff, B. Ziegler, H. W. Koch, and R. Uhlig, Phys. Rev. 137, B576 (1965).
- ³³Y. Torizuka, Y. Kojima, T. Saito, K. Itoh, A. Nakada, S. Mitsunobu, M. Nagao, K. Hosoyama, S. Fukuda, and H. Miura, in *Photoneuclear Reactions and Applications*, edited by B. L. Berman (Lawrence Livermore Laboratory, Livermore, California, 1973), Vol. I, p. 675.
- ³⁴N. Marty, M. Morlet, A. Willis, V. Comparat, and R. Frascaria, Nucl. Phys. A238, 93 (1975).
- ³⁵J. Arvieux, M. Buenerd, A. J. Cole, P. de Saintignon, G. Perrin, and D. J. Horen, Nucl. Phys. A247, 238 (1975).
- ³⁶F. P. Brady, N. S. P. King, M. W. McNaughton, and G. R. Satchler, Phys. Rev. Lett. 36, 15 (1976).
- ³⁷H. P. Morsch, P. Decowski, and W. Benenson, Phys. Rev. Lett. 37, 263 (1976).
- ³⁸H. W. Bertini, G. D. Harp, and F. E. Bertrand, Phys. Rev. C 10, 2472 (1974).
- ³⁹J. N. Palmieri, A. M. Cormack, N. F. Ramsey, and R. Wilson, Ann. Phys. (N. Y.) 5, 299 (1958).
- ⁴⁰A. Willis, B. Geoffrion, N. Marty, M. Morlet, C. Roland, and B. Tatischeff, Nucl. Phys. A112, 417 (1968).
- ⁴¹A. Willis, B. Geoffrion, N. Marty, M. Morlet, and B. Tatischeff, J. Phys. (Paris) 30, 13 (1969).
- ⁴²H. Sherif and J. S. Blair, Nucl. Phys. A140, 33 (1970).
- ⁴³A. Ingemarsson, E. Hagberg, and H. Sherif, Nucl. Phys. A216, 271 (1973).
- ⁴⁴N. Austern, *Direct Nuclear Reaction Theories* (Wiley, New York, 1970).
- ⁴⁵W. B. Riesenfeld and K. M. Watson, Phys. Rev. 102, 1157 (1956).
- ⁴⁶M. P. Fricke, E. E. Gross, B. J. Morton, and A. Zucker, Phys. Rev. 156, 1207 (1967).
- ⁴⁷F. D. Becchetti, Jr., and G. W. Greenlees, Phys. Rev. 182, 1190 (1969).
- ⁴⁸S. Fernbach, W. Heckrotte, and J. V. Lepore, Phys. Rev. 97, 1059 (1955).
- ⁴⁹R. M. Haybron and H. M. McManus, Phys. Rev. 140, B638 (1965).
- ⁵⁰E. C. Halbert, J. B. McGrory, G. R. Satchler, and J. Speth, Nucl. Phys. A245, 189 (1975).
- ⁵¹G. R. Hammerstein, H. McManus, A. Moalem, and T. T. S. Kuo, Phys. Lett. 49B, 235 (1974).
- ⁵²D. H. Jakubassa, Z. Phys. 268, 409 (1974).
- ⁵³F. E. Bertrand and D. C. Kocher, Phys. Rev. C 13, 2241 (1976).